DEPARTURE TRAJECTORY OPTIMIZATION FOR NOISE ABATEMENT PROCEDURE IN SOEKARNO-HATTA INTERNATIONAL AIRPORT

Vincentius N.S. Suryo[1], Benedikt Grüter[2], Johannes Diepolder[3], Neno Ruseno[4], and Florian Holzapfel[5]

[1,4]Aviation Engineering Department, International University Liaison Indonesia

[1,2,3,5]Institute of Flight System Dynamics, Technische Universität München

[4]E-mail: neno.ruseno@iuli.ac.id

Received: 16 July 2020; Revision: 10 August 2020; Accepted :

ABSTRACT

Air traffic noise emission has been a growing concern for communities living within the vicinity of airports due to a massive increase in air traffic volume in recent years. This work focuses on the noise annoyance problem by optimizing one of the RNAV trajectories, which aims to minimize the noise footprint of a flying aircraft in a low altitude trajectory. Optimal control theory is applied to minimize the number of awakenings caused by a departing aircraft while constraining the relative increase of fuel consumption with regard to a fuel-minimal trajectory. The aircraft simulation model is based on the BADA 3 database, while the noise is modeled according to the ANP database, both published by EUROCONTROL. The methodology is demonstrated for the Soekarno-Hatta International Airport (CGK) in Jakarta; the result shows the comparison between fuel-minimal trajectories and noise-minimal trajectories for seven aircraft types representing the fleet mix at CGK. The number of awakenings of the noise-minimal trajectories is reduced by 30.33%, with an additional of 5% fuel consumption for the seven aircraft types when compared to the fuel-minimal trajectory.

Keywords: *Optimal Control Theory, Noise Abatement, Trajectory Optimization, RNAV Trajectory, BADA Database, Departure Trajectories.*

1 Introduction

Due to the continuous growth of air traffic, noise annoyance has become an increasing concern, especially in the vicinity of airports. Despite many advancements in technology to significantly reduce noise emissions, the level of noise disturbances has remained unchanged or even increased due to the increase in the number of movements (landing or takeoff). Research from the Aviation Environment Federation (AEF) has shown that extensive exposure to noise can cause health problems such as cardiovascular diseases, sleep disturbance and is even has an impact of learning on children (AEF, 2016).

This work focuses on the Noise Abatement Procedures (NAP), which manipulate flight paths of an aircraft, whether in the lateral flight path or vertical flight path. The procedure applied to the Soekarno-Hatta International Airport (CGK) using one of the Standard Instrument Departure (SID) procedures waypoints existing in the airport.

For this case study, fuel and noise optimal trajectories are obtained by applying Optimal Control Theory (OCT). OCT has been used previously in the context of noise abatement by Xavier Prats (Prats, et al., 2010) to optimize noise for the Girona Airport in Spain.

Similar works are the developments of advanced operational procedures framework to analyze noise impacts by Thomas (Thomas & Hansman, 2019), strategy to design NAP by implementing nonlinear multi-objective optimal control problem by Prats (Prats, et al., 2010), performance bounding of continuous descent arrival procedures in terms of operating costs by Park (Park & Clarke, 2015), optimization tool for departure noise abatement procedure by using reference flight path by Wijnen (Wijnen & Visser, 2003), design of aircraft terminal routes for noise abatement by employing a multi-objective evolutionary algorithm based on decomposition by Ho-Huu (Ho-Huu, et al., 2018), and determination of noise-minimal departure trajectories by Richter (Richter, et al., 2014). This paper extends previous work applicability, where it uses similar methodologies to be applied for one airport, contributing to noise emission reduction.

2 Methodology

The research focuses on applying OCT for a CGK SID departure trajectory. The following subsections present the Optimal Control Problem (OCP) formulation, the noise disturbance cost function, the scenario definition, and the aircraft simulation model.

2.1. Optimal Control Theory

The OCP is formulated as a Bolza-type objective function J consisting both of the Mayer Term (θ) and Lagrange Term ($\mathcal{L}$). The Bolza-type problem is formulated as follows (Prats, et al., 2006):

$$\min J = \theta\left(\boldsymbol{x}(t_0), \boldsymbol{x}(t_f)\right) + \int_{t_0}^{t_f} \mathcal{L}(\boldsymbol{x}, \boldsymbol{u}) dt \quad (2\text{-}1)$$

subject to:

Dynamic Constraints

$$\dot{\boldsymbol{x}} = f(\boldsymbol{x}, \boldsymbol{u}) \quad (2\text{-}2)$$

Event Constraints

$$\phi_{min} \leq \phi\left(\boldsymbol{x}(t_0), t_0, \boldsymbol{x}(t_f)\right) \leq \phi_{max} \quad (2\text{-}3)$$

Path Constraints

$$\boldsymbol{h}_{min} \leq \boldsymbol{h}(\boldsymbol{x}, \boldsymbol{u}) \leq \boldsymbol{h}_{max} \quad (2\text{-}4)$$

where $\boldsymbol{x}(t) \in \mathbb{R}^m$ is the state vector, $\boldsymbol{u}(t) \in \mathbb{R}^n$ is the control vector, t_0 is the initial time, and t_f is the final time, which is set to be free. The fuel-minimum trajectories problem is formulated as a Mayer-type problem with:

$$\theta\left(\boldsymbol{x}(t_0), \boldsymbol{x}(t_f)\right) = -m(t_f) \quad (2\text{-}5)$$

where $m(t_f)$ is the mass of the aircraft at the end of the optimization. While the noise-minimum trajectory is formulated as Lagrange-type problem with:

$$\int_{t_0}^{t_f} \mathcal{L}(\boldsymbol{x}, \boldsymbol{u}) dt = N_{awak} \quad (2\text{-}6)$$

where N_{awak} is the number of awakenings, to be explained in subsection 2.2. The optimization process uses a combined objective function consisting of fuel and noise. Therefore, the resulting trajectory should converge to a point where neither objective can be improved without worsening the other, better known as Pareto optimality condition (Chatterjee, 2011). The epsilon-constraint ($\epsilon - constraint$) method is chosen to obtain points fulfilling the Pareto optimality condition, based on (Haimes, et al., 1971), where:

Problem A	$\min\left[-m(t_f), N_{awak}\right]$
subject to	$\boldsymbol{g}(\boldsymbol{x},\boldsymbol{u}) \leq 0$

is replaced by

Problem B (ϵ)	$\min N_{awak}$
subject to	$\Delta r_{fuel} \leq \epsilon$
	$\boldsymbol{g}(\boldsymbol{x},\boldsymbol{u}) \leq 0$

where $\boldsymbol{g}(\boldsymbol{x},\boldsymbol{u}) \leq 0$ collects all constraints of the optimal control problem and Δr_{fuel} represents the relative additional fuel consumption, computed in subsection 2.2. Applying this method, we can choose any value of ϵ to be employed as an additional constraint for fuel consumption when solving the noise minimization problem, explained in subsection 2.2.

The method chosen to solve the Bolza problem is the trapezoidal collocation method. The trapezoidal collocation works by converting a continuous-time OCP into a nonlinear program using trapezoidal quadrature to replace the continuous solution to the differential equation by a discrete approximation (Kelly, 2017). Furthermore, the optimal control toolbox called FALCON.m was used in this study (Rieck, et al., n.d.).

2.2. Objective Function

The Sound Exposure Level (SEL) objective function must be defined before the scenario definition. The research conducted by Figlar (Miller & Gardner, 2008) yields a differentiable model for the sound pressure level L_A:

$$L_A = c_0 + c_1 T_{corr} + c_2 \log(d) + c_3 \log(d)^2 \quad (2\text{-}7)$$

The coefficients c_0, c_1, c_2 and c_3 are specific to the aircraft type and can be estimated using the Aircraft Noise and Performance (ANP) database published by EUROCONTROL (EUROCONTROL, 2020). T_{corr} is the corrected net thrust of the engine, and d is the distance between a noise receiver and an aircraft. The sound pressure level is integrated over the period in which the aircraft travels to the specific location yielding SEL:

$$SEL = \int_{t_0}^{t_f} 10^{0.1 \cdot L_A(t)}\, dt \quad (2\text{-}8)$$

The resulting SEL is used to estimate the expected probability of a person awakening due to noise exposure (P_{awak}) in a particular location, which can be calculated by using the ANSI Curve Sleep Standard for single events (Miller & Gardner, 2008):

$$P_{awak} = \frac{1}{1+e^{-Z}} \quad (2\text{-}9)$$

Where

$$Z = \beta_0 + \beta_L \cdot SEL + \beta_T \cdot T_{retire} + \beta_S \cdot S_{sensitivity} \quad (2\text{-}10)$$

And

$\beta_0, \beta_L, \beta_T, \beta_S$ = constant
T_{retire} = Time since retiring, minutes
$S_{sensitivity}$ = Sensitivity for population segment

For this case study, the percentage of awakenings is computed as a function of SEL only, therefore, T_{retire} and $S_{sensitivity}$ is assumed to be zero. In this case, the constants value of β_0 and β_L are -6.8884 and 0.0444, respectively. Further explanation can be found in (Miller & Gardner, 2008). The resulting P_{awak} are used to calculate the number of awakenings (N_{awak}) in each location by multiplying the value with the number of inhabitants $w_{R,i}$:

$$N_{awak} = \sum_{i=1}^{n} P_{awak,i} \cdot w_{R,i} \quad (2\text{-}11)$$

where the index i represents the number of each receiver, and n is the total number of receivers. The other objective function to be optimized is the final mass of the aircraft $m(t_f)$. We want to maximize $m(t_f)$ so that the fuel consumption defined by the difference between initial and final mass is minimized. As explained in subsection 2.1, the epsilon-constraint method is employed to restrict the relative additional fuel consumption when minimizing noise. The epsilon-constraint value can be determined by:

$$\Delta r_{fuel} = \frac{m(t_0) - m(t_f)}{m(t_0) - m^*(t_f)} - 1 \leq \epsilon \qquad (2\text{-}12)$$

where the nominator represents the noise-minimal trajectory's fuel consumption, and the denominator represents the fuel-minimal trajectory's fuel consumption. This work uses different values of ϵ: 0.0, 0.025, 0.05, and 0.075, to determine the trend of the number of awakenings N_{awak} in correspondence with different relative additional fuel consumption.

2.3. Aircraft Model Description

This subsection discusses the aircraft types chosen for this research as well as the reason behind the decision. There are seven types of aircraft which is considered in the optimization, consisting of four narrow-body jet airliner B737-800NG (B738), B737-500CL (B735), B737-900NG (B739), A320-200 (A320), two wide-body jet airliner A330-200 (A332) and B777-300 (B773), and one regional jet CRJ-900 (CRJ9). According to the Blue Swan daily (The Blue Swan Daily, 2018), the seven types are the most frequent aircraft types flying into and out of the Soekarno-Hatta International Airport, making up over 90% of movements at the airport in domestic and international flights, which is shown in Figure 2-1.

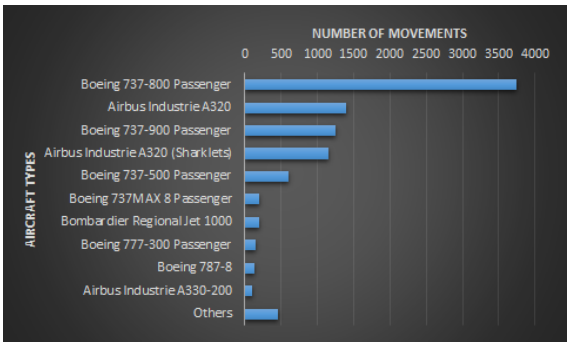

Figure 2-1: Aircraft Movement in CGK in 2018 (The Blue Swan Daily, 2018)

The aircraft model is built according to the Base of Aircraft Data Family 3 (BADA3) published by EUROCONTROL (Nuic, et al., 2010). Its performance characteristics are taken from the Aircraft Performance Database (APD), also published by EUROCONTROL (EUROCONTROL Experimental Centre, n.d.).

2.4. Scenario Definition

The southeast bound departure procedure of runway 25R is the basis of the optimization scenario in this research. Figure 2-2 shows the CA1D Standard Instrument Departure (SID) procedure. The procedure has an initial climb on the runway heading up to 8,000 feet and turns right directly to waypoint NABIL after reaching 500 feet upon lift-off. From this point, the aircraft turns right after NABIL to 113-degree radial heading towards NANTO, maintaining its altitude at 8,000 feet. It continues this heading until 'CA' NDB while climbing continuously up to 18,000 feet at MUTIA and 24,000 feet at 'CA' NDB (Jeppesen Sanderson Inc., 2018).

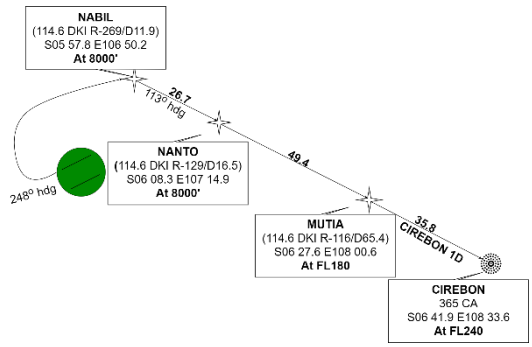

Figure 2-2: CA1D SID Departure (Jeppesen Sanderson Inc., 2018)

The Optimization process in the departure trajectory is focusing on the initial climb starting from the runway threshold when the aircraft takeoff at the speed of v_2, until the waypoint NABIL at 8,000 feet or 2,440 m high from the sea level. The reason behind this scenario is because, after the waypoint NABIL in CA1D SID, the aircraft has reached a sufficient altitude that the noise produced has little effect on the populated area below it. The origin point of this scenario is the threshold of runway 25R, and subsequently, all the reference positions of populated areas, as well as the position of NABIL waypoint, are measured relative to this origin point. The coordinates of runway 25R and waypoint NABIL, NANTO, MUTIA, and CA NDB are given in Table 2-1.

We compute the relative distance of each waypoint to the runway 25R by using the geodetic conversion formula in the North-East-Down (NED) frame. The relative distance of the last waypoint is to be used as the final boundary condition of the departure trajectory, which in this case, is NABIL waypoint.

The locations which are considered as receivers are the western, central, and eastern parts of the city of Jakarta, Cengkareng region, and some parts of South Tangerang City. These areas are located within 20 kilometers of CGK, where aircraft flies below 8,000 feet with almost full thrust power, resulting in very high noise in the area. The location area is shown in Figure 2-3.

Table 2-1: Waypoints Coordinates (Directorate General of Civil Aviation Indonesia, 2019)

Waypoints	Latitude	Longitude
RWY 25R	[S06 06 32.27]	[E106 40 08.62]
NABIL	[S05 57 47.96]	[E106 50 13.48]
NANTO	[S06 08 17.14]	[E107 14 54.04]
MUTIA	[S06 27 34.25]	[E108 00 33.53]
CA NDB	[S06 41 52.73]	[E108 33 35.13]

Figure 2-3: Receivers for Noise Abatement (Source: Google Earth, ©2020 Google, ©2020 Maxar Technologies)

The receivers' location is gridded per kilometer-square, and each kilometer-square is filled with a particular population number which is extracted from the "Gridded Population of the World (GPW), v4" published by the Socioeconomic Data and Applications Center (SEDAC) at Columbia University (Columbia University, n.d.). The latitude and longitude limits of the receivers' area are shown in Table 2-2.

Table 2-2: Latitude and Longitude for the Receiver's Area Limit.

Limit Position	Latitude Limit [D M S]	Longitude Limit [D M S]
Lower Left	[S06 13 05.88]	[E106 30 24.84]
Lower Right	[S06 13 05.88]	[E106 54 12.96]
Upper Left	[S05 51 48.24]	[E106 30 24.84]
Upper Right	[S05 51 48.24]	[E106 54 12.96]

The resulting gridded populated area with its population number is shown in Figure 2-4, where the color map represents the population density in one kilometer-square area.

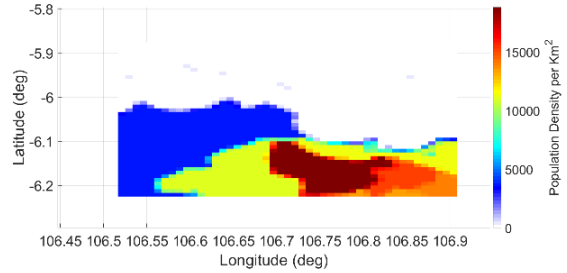

Figure 2-4: Population Area Density

2.5. Problem Formulation

The dynamic model and problem formulation are discussed in this subsection. There are eight states and three control variables within the problem. Writing the states and controls in vector form yield:

$$\boldsymbol{x} = \begin{bmatrix} \boldsymbol{n} \\ \boldsymbol{e} \\ \boldsymbol{d} \\ \boldsymbol{v} \\ \boldsymbol{\chi} \\ \boldsymbol{\gamma} \\ \boldsymbol{\delta_T} \\ \boldsymbol{m} \end{bmatrix} \quad (2\text{-}13)$$

$$\boldsymbol{u} = \begin{bmatrix} \boldsymbol{\alpha} \\ \boldsymbol{\delta_{T,cmd}} \\ \boldsymbol{\mu} \end{bmatrix} \quad (2\text{-}14)$$

The first three states, $\boldsymbol{n}, \boldsymbol{e},$ and $\boldsymbol{d}$ are the 3D spatial representation of the aircraft in the NED-frame, $\boldsymbol{v}$ is the absolute velocity, $\boldsymbol{\chi}$ is the course angle, $\boldsymbol{\gamma}$ is the climb angle, $\boldsymbol{\delta_T}$ is the thrust lever position, $\boldsymbol{\delta_{T,cmd}}$ is the commanded thrust lever position, $\boldsymbol{m}$ is the mass of the aircraft, $\boldsymbol{\alpha}$ is the angle of attack, and $\boldsymbol{\mu}$ is the bank angle. Then, we introduce the output of this model as:

$$\boldsymbol{Y} = \begin{bmatrix} \boldsymbol{n_z} \\ \boldsymbol{h} \\ \boldsymbol{h_{dot}} \\ \boldsymbol{T} \end{bmatrix} \quad (2\text{-}15)$$

where $\boldsymbol{n_z}$ is the load factor in the $\boldsymbol{z}$-direction of the body frame, $\boldsymbol{h}$ is the aircraft's height above the reference ellipsoid, $\boldsymbol{h_{dot}}$ is the kinematic vertical speed corresponding to $\boldsymbol{h}$, and $\boldsymbol{T}$ is the absolute thrust value in which the value is dependent on the aircraft types. The dynamic equations governing the evolution of the states are:

$$\begin{bmatrix} \dot{\boldsymbol{n}} \\ \dot{\boldsymbol{e}} \\ \dot{\boldsymbol{d}} \end{bmatrix}_{\boldsymbol{O}}^{\boldsymbol{E}} = \boldsymbol{\mathcal{R}_{OK}} \cdot \begin{bmatrix} \boldsymbol{v} \\ \boldsymbol{0} \\ \boldsymbol{0} \end{bmatrix}_{\boldsymbol{K}} \quad (2\text{-}16)$$

$$\begin{bmatrix} \dot{\boldsymbol{v}} \\ \dot{\boldsymbol{\chi}} \\ \dot{\boldsymbol{\gamma}} \end{bmatrix} = \begin{bmatrix} \boldsymbol{1} & \boldsymbol{0} & \boldsymbol{0} \\ \boldsymbol{0} & \frac{\boldsymbol{1}}{\boldsymbol{v \cdot \cos(\gamma)}} & \boldsymbol{0} \\ \boldsymbol{0} & \boldsymbol{0} & -\frac{\boldsymbol{1}}{\boldsymbol{v}} \end{bmatrix} \cdot \frac{\boldsymbol{1}}{\boldsymbol{m}} \sum(\boldsymbol{F})_{\boldsymbol{K}} \quad (2\text{-}17)$$

$$\dot{\delta_T} = \frac{1}{T_T} \cdot (\delta_{T,cmd} - \delta_T) \quad (2\text{-}18)$$

$$\dot{m} = -\dot{m}_f \cdot (\boldsymbol{F}_P, h, v, \rho) \quad (2\text{-}19)$$

In which $\boldsymbol{\mathcal{R}_{OK}}$ is the coordinate transformation matrix from kinematic frame to NED frame, h is the altitude, ρ is the Atmospheric air density based on the International Standard Atmosphere

(ISA), and $\sum(\boldsymbol{F})_K$ is the summation of forces in the kinematic frame given by (Gerdts & Grüter, 2019):

$$\sum(\boldsymbol{F})_K = \boldsymbol{\mathcal{R}}_{KO}\boldsymbol{\mathcal{R}}_{OA}(\boldsymbol{F_A})_A + \boldsymbol{\mathcal{R}}_{KB}(\boldsymbol{F_P})_B + \boldsymbol{\mathcal{R}}_{KB}(\boldsymbol{F_P})_B + \boldsymbol{\mathcal{R}}_{KO}(\boldsymbol{F_G})_O \quad (2\text{-}20)$$

In which $\boldsymbol{\mathcal{R}}_{KO}$ is the coordinate transformation from NED frame to kinematic frame, $\boldsymbol{\mathcal{R}}_{OA}$ is the coordinate transformation matrix from aerodynamic frame to NED frame, and $\boldsymbol{\mathcal{R}}_{KB}$ is the coordinate transformation matrix from the body frame to the kinematic frame. The force vector $\boldsymbol{F_A}, \boldsymbol{F_P}, \boldsymbol{F_G}$ stands for aerodynamic, propulsion, and gravitation force, respectively, and are given by:

$$\boldsymbol{F_A} = \begin{bmatrix} -D \\ 0 \\ -L \end{bmatrix}_A \quad (2\text{-}21)$$

$$\boldsymbol{F_P} = \begin{bmatrix} T \\ 0 \\ 0 \end{bmatrix}_B \quad (2\text{-}22)$$

$$\boldsymbol{F_G} = \begin{bmatrix} 0 \\ 0 \\ m \cdot g \end{bmatrix}_O \quad (2\text{-}23)$$

In which D is the drag force, L is the lift force, T is the thrust output, m is mass of the aircraft, and g is Earth's gravitational acceleration.

3. Results

The result compares the fuel minimization trajectories for all aircraft types (trajectory 1) with the fuel/noise optimization trajectories for all aircraft types included in this research (trajectory 2). Trajectory 1 uses the aircraft's mass as its objective to be maximized, and the resulting minimum fuel consumption is used for fuel consumption benchmark in trajectory 2. On the other hand, trajectory 2 uses the number of awakenings as its objective to be minimized, and the epsilon constraint is applied to restrict the additional fuel consumption. The values chosen for the epsilon constraint are 0.025 (2.5%), 0.05 (5%), and 0.075 (7.5%) additional fuel to see the impact of fuel to the number of awakenings.

In general, trajectories 1 follow RNAV guidelines where after takeoff, the aircraft takes a right turn immediately and flies straight towards NABIL. Also, all aircraft types take similar fuel minimal trajectories except for CRJ9 and B773, which exhibit larger radii. On the other hand, trajectories 2 display a different approach towards NABIL. After takeoff, they avoid the densely populated areas first before flying towards NABIL, resulting in larger turning radii for all aircraft types. The resulting trajectories are shown in Figure 3-1, where the solid lines represent trajectories 1, the dotted lines represent trajectories 2 with 5% additional fuel, and the gridded population area is shown as a contour plot with its population density as the color map.

Figure 3-2 summarizes the parameters and objective function values for both trajectories, in which a similar pattern of increasing time and fuel noise while the decreasing number of awakenings can be found for all aircraft types. Principally, the time to fly trajectories 1 is about 252 seconds on average, while it took 291 seconds to fly trajectories 2 for the seven aircraft types. Additionally, all aircrafts' fuel consumption in trajectory 2 fulfilled the requirement of the epsilon-constraint. Figure 3-2 also shows the parameter of trajectory 2 when using 2.5% and 7.5% additional fuel restriction.

Looking into each aircraft class type, the narrow-body jets, A320, B735, B738, and B739 yield similar parameters in terms of time taken to fly both

trajectories. The four aircraft types result in 235 seconds for minimum fuel trajectory, 245 seconds for 2.5% additional fuel, 257 seconds for 5.0% additional fuel, and 271 seconds for 7.5% additional fuel. For the four aircraft types, every 2.5% additional fuel result in 5% relative additional time on average.

In terms of fuel consumption, the narrow-body airliners also have similar minimum fuel consumption. The minimum fuel consumption values are 386 kg for A320, 416 kg for B735, and 422 kg for both B738 and B739. The fuel consumption rises according to the epsilon constraint value.

In terms of noise exposure, however, the four types show different values compared to each other. For the minimum fuel trajectory, the average number of awakenings varies from 136 (A320) to 278 people (B739), while B735 and B738 yield 152 and 244 number of awakenings, respectively. Compared to the fuel-minimal trajectory, the four types have a significant reduction in terms of the number of awakenings. With 2.5% additional fuel, the number of awakenings for the four types reduces by 32.8% on average, 36.4% for 5% additional fuel, and 38.6% for 7.5% additional fuel. The B739, in particular, has the highest reduction regarding the number of awakenings among the narrow-body airliner aircraft types, reaching nearly 50% reduction for 5% additional fuel consumed compared to the number of awakenings in minimum fuel trajectory.

The two wide-body airliner types, the A332 and B773, exhibit similar patterns in their trajectories. In terms of time taken, the A332 takes 237 seconds for the fuel-minimal trajectory, and B773 takes 310 seconds for the same trajectory. When solving for noise and the epsilon constraint is applied, both types have an increase of flying time at about 4.7% for every 2.5% relative additional fuel is consumed. The trajectory 1 fuel consumption for A332 and B773 is 1106 and 1663 kg, respectively, and it changes according to the fuel restriction for trajectory 2.

The number of awakenings for the wide-body airliner is fairly surprising. The number of awakenings in the fuel-minimal trajectory for A332 is 201 people. This value is lower than that which is seen for B738 and B739. The B773 also has a lower number of awakenings value, 163 people, than the narrow airliner types due to a larger turn radius in its fuel-minimal trajectory, which in turn flying above a sparsely populated area. As a result, the reductions for the wide-body aircraft types are not as significant as those for the narrow-body airliners. The number of awakenings' reduction for A332 are 23.4%, 28.4%, and 30.9% for 2.5%, 5%, and 7.5% additional fuel, respectively. For B773, the reduction is lesser, yielding only 1.2%, 2.5%, and 3.7%, respectively, for the same additional fuel consumption.

The last aircraft type, CRJ9, has some unusual parameters. The flying time increases by 15% for every 2.5% increment of additional fuel consumption. This increase is more significant when compared to other aircraft types. The baseline fuel consumption for CRJ9 is 150 kg and increases accordingly to the epsilon constraint. For the fuel-minimal trajectory, CRJ9 has the number of awakenings value of 93 people. This value diminishes to 52, 49, and 49 people for 2.5%, 5%, and 7.5% additional fuel, a reduction worth of 46.2% on average for the type.

In summary, with 5.0% relative additional fuel, all aircraft types shows a reduction of the number of awakenings as follows: 25.74% for A320, 28.36% for A332, 23.03% for B735, 36.89% for B738, 48.56% for B739, 2.45% for B773, and 47.31% for CRJ9. These values result in an averagely 30.33% number of awakenings reduction for the seven aircraft types.

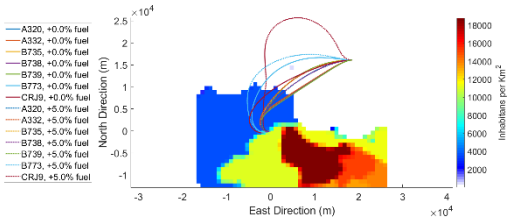

Figure 3-1:Different Aircraft Types Trajectory for Fuel/Noise Optimization

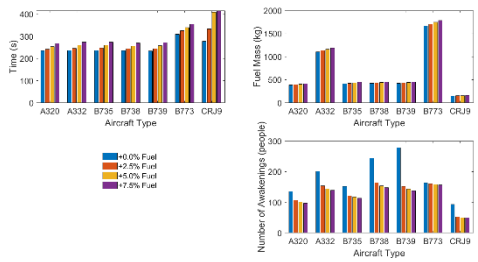

Figure 3-2:Trajectory Data for different Aircraft Types (Top-Left: Time Parameter, Top-Right: Fuel Consumption, Bottom-Right: Number of Awakenings)

The B739's noise footprint is discussed in detail since it produces the highest noise exposure among the seven aircraft types, whereas all noise footprints of the other aircraft types are provided in appendix A. Figure 3-3 shows the noise footprint in terms of SEL for the B739 aircraft. The top picture is the SEL footprint of the fuel-minimal trajectory (trajectory 1), and the bottom picture is for the noise-minimal trajectory (trajectory 2) with 5.0% additional fuel consumption. The most significant exposure happens at the start of the trajectory where the aircraft applies its full thrust, and due to its low altitude, the noise exposure level reaches its highest at about 130 dB in this area. As the aircraft climbs and reduces its thrust output progressively, the SEL reduces in the greater area accordingly. Trajectory 2, in turn, trades off noise levels with fuel consumption. the second part of Figure 3-3 shows the highest noise levels when using an additional 5.0% fuel consumption yields about 100 dB at the start of the trajectory instead of 130 dB. This result then affects the overall noise levels on the trajectory, which is lower than that in trajectory 2.

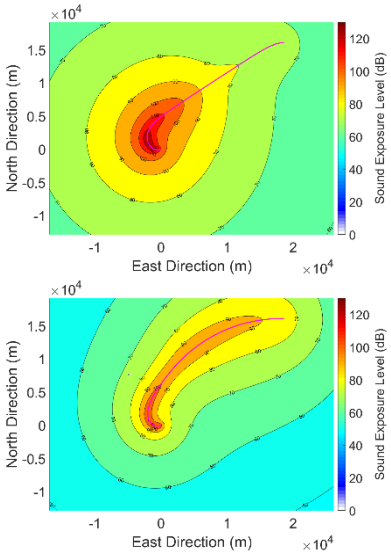

Figure 3-3:Sound Exposure Level Footprint for B739 (Top: +0.0% Fuel-minimal Trajectory, Bottom: +5.0% fuel Noise-minimal Trajectory)

The number of awakenings (Figure 3-4) due to a departing B739 is profoundly affected by the population density in the area (Figure 2-4) and the sound exposure level (Figure 3-3). For trajectory 1, even when the southeast area gets exposed to a similar level of noise, it yields in a higher number of awakenings than the northwest area due

to its high-density inhabitants, with the highest number yields as high as 1,200 people. Trajectory 2 then avoided these high-density areas as much as possible, resulting in lower noise and awakenings percentage to the area. Hence, the same area which previously had between 1,000 and 1,200people awakened now is reduced to about 400 to 800 people.

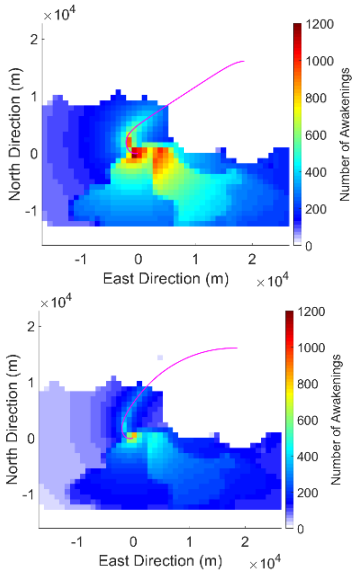

Figure 3-4:Number of Awakenings Footprint for B739 (Top: +0.0% Fuel-minimal Trajectory, Bottom: +5.0% fuel Noise-minimal Trajectory)

4 Conclusions

OCT has been successfully applied to generate noise-optimized trajectories on the airport, in which the resulting trajectories have been discussed in detail. The results regarding the departure trajectories indicate a potential reduction of the average number of awakenings by 30.33% for 5% additional fuel consumption in the seven aircraft types, benefitting the environments by reducing noise emissions. It is important to note that although the research methodology is applied for the Soekarno-Hatta International Airport in Jakarta geographically, the research method can be applied in any airport. Furthermore, the algorithm used in this research can also be applied to any aircraft types, making it a generic algorithm that can be adapted in any airport and aircraft. Therefore, the methodology of the research can be used for a tool to plan SIDs in airports worldwide.

The research results in new noise-minimization trajectories for one RNAV procedure in the departure scenario. It would be interesting to see other RNAV procedures of this airport go through the same process of noise optimization to see a significant reduction in noise emission. Also, the scope of this work is applied for one aircraft at a time. It is intriguing to see multiple aircrafts operation and see the resulting noise footprints for the area below it. Nevertheless, the application of OCT to minimize noise by generating new trajectories contributes to a further sustainable aircraft operation in terms of noise exposure.

Acknowledgments

The authors would like to give their gratitude to all parties involved in supporting this research, who, directly and indirectly, have lent their hand in this research work.

The authors also take this opportunity to be grateful to all of the Department faculty members for their share of knowledge, help, and support.

Contributorship Statements

Vincentius N.S. Suryo (VS) is the main contributor of this manuscript. VS made the research concept and planning as well as finding references and solving the research problem. Benedikt Grüter (BG) and Johannes Diepolder (JD) provided the tool to conduct the research as well as compiling the

necessary data required to the research. Neno Ruseno (NR) helped with the verification and validation of the research results as an internal reviewer. Lastly, Florian Holzapfel (FH) provided the research group with authorization and final approval for the manuscript to be published.

References

AEF, (2016). Aircraft Noise and Public Health: The Evidence is Loud and Clear.[Online] Available at: https://www.aef.org.uk/uploads/Aircraft-Noise-and-Public-Health-the-evidence-is-loud-and-clear-final-reportONLINE.pdf [Accessed 21 August 2019].

Chatterjee, D. K., (2011). Encyclopedia of Global Justice. Dordrecht: Springer Netherlands. DOI: 10.1007/978-1-4020-9160-5.

Columbia University, n.d. Gridded Population of the World (GPW), v4 | SEDAC.[Online] Available at: https://sedac.ciesin.columbia.edu/data/collection/gpw-v4 [Accessed 6 March 2020].

Directorate General of Civil Aviation Indonesia, 2019. AIP Indonesia (VOL II) WIII AMDT 76. [Online] Available at: https://aimindonesia.dephub.go.id/index.php?page=product-aip-electronik-vol123.html&id_aip=119 [Accessed 18 September 2019].

EUROCONTROL Experimental Centre, n.d. Aircraft Performance Database. [Online] Available at: https://contentzone.eurocontrol.int/aircraftperformance/default.aspx? [Accessed 12 February 2020].

EUROCONTROL, (2020). ANP - Eurocontrol Experimental Centre. [Online] Available at: https://www.aircraftnoisemodel.org/[Accessed 12 September 2019].

Gerdts, M. & Grüter, B., (2019). Aircraft Trajectory Optimization, München: Lehrstuhl für Flugsystemdynamik.

Haimes, Y. Y., Lasdon, L. S. & Wismer, D. A., 1971. On a Bicriterion Formulation of the Problems of Integrated System Identification and System Optimization. IEEE Transactions on Systems, Man, and Cybernetics, SMC-1(3), pp. 296 - 297.DOI: 10.1109/TSMC.1971.4308298.

Ho-Huu, V. et al., (2018). Optimization of noise abatement aircraft terminal routes using a multi-objective evolutionary algorithm based on decomposition. Transportation Research Procedia, Volume 29, pp. 157-168.DOI: 10.1016/j.trpro.2018.02.014.

Jeppesen Sanderson Inc., (2018). Airport Information for WIII, Englewood: s.n.

Kelly, M., (2017). An Introduction to Trajectory Optimization: How to Do Your Own Direct Collocation. Society for Industrial and Applied Mathematics (SIAM) Review, 59(4), pp.849-904.DOI: 10.1137/16M1062569.

Miller, N. P. & Gardner, C. R., (2008). How Many people will be awakened by Night time Aircraft Noise?. Foxwoods, 9th International Congress on Noise as a Public Health Problem (ICBEN), pp. 1 - 8..

Nuic, A., Poles, D. & Mouillet, V., (2010). BADA: An advanced aircraft performance model for present and future ATM systems. International Journal of Adaptive Control and Signal Processing, 24(10), p. 850–866. DOI: 10.1002/acs.1176.

Park, S. G. & Clarke, J.-P., (2015). Optimal Control Based Vertical Trajectory Determination for Continuous Descent Arrival Procedures. Journal of Aircraft,

September, 52(5), pp. 1469-1480. DOI: 10.2514/1.C032967.

Prats, X. et al., (2006). A Framework for RNAV Trajectory Generation Minimizing Noise Nuisances. pp. 1 - 10.Retrievedfrom: https://core.ac.uk/download/pdf/41755854.pdf.

Prats, X., Puig, V. & Quevedo, J., (2010). A Multi-Objective Optimization Strategy for Designing Aircraft Noise Abatement Procedures. Case Study at Girona Airport. Transportation Research Part D, 16(1), pp. 31 - 41. DOI: 10.1016/j.trd.2010.07.007.

Prats, X., Puig, V., Quevedo, J. & Nejjari, F., (2010). Multi-Objective Optimization for Aircraft Departure Trajectories Minimizing Noise Annoyance. Transportation Research Part C, 18(6), pp. 975 - 989.DOI: 10.1016/j.trc.2010.03.001.

Richter, M., Bittner, M., Rieck, M. & Holzapfel, F., (2014). A Non-Cooperative Bi-Level Optimal Control Problem Formulation for Noise Minimal Departure Trajectories. 29th Congress of the International Council of the Aeronautical Sciences, pp. 1 - 7.

Rieck, M. et al., n.d. FALCON.m | TUM – Institute of Flight System Dynamics –Software.[Online] Available at: https://www.fsd.lrg.tum.de/software/falcon-m/ [Accessed 7 August 2019].

The Blue Swan Daily, (2018). Airport Insight: Jakarta Soekarno-Hatta International Airport – Blue Swan Daily.[Online] Available at: https://blueswandaily.com/airport-insight-jakarta-soekarno-hatta-international-airport/ [Accessed 12 August 2019].

Thomas, J. L. & Hansman, R. J., (2019). Framework for Analyzing Aircraft Community Noise Impacts of Advanced Operational Flight Procedures. Journal of Aircraft, 56(4), pp. 1407 - 1417. DOI: 10.2514/1.C035100.

Wijnen, R. & Visser, H., (2003). Optimal Departure Trajectories with respect to Sleep Disturbance. Aerospace Science and Technology, 7(1), pp. 81 - 91. DOI: 10.1016/S1270-9638(02)01183-5.

Appendix A: Noise Footprint Figures

- A320 Noise Footprint

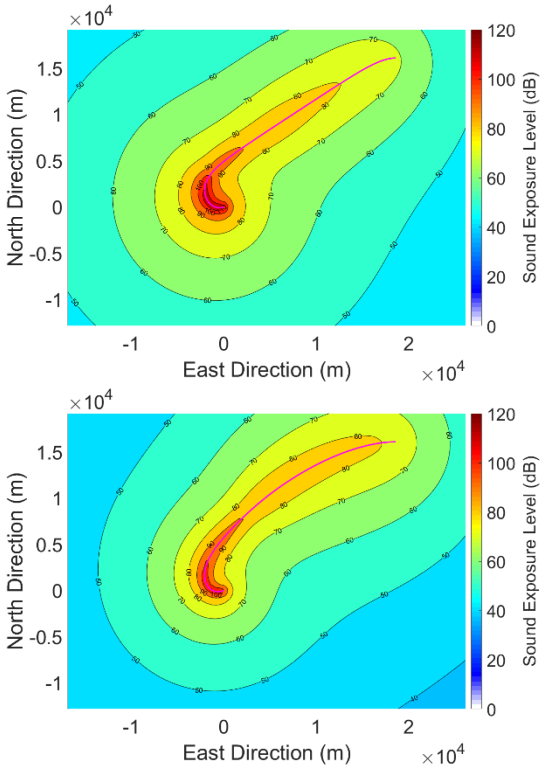

Figure A-1: Sound Exposure Level Footprint for A320 (Top: +0.0% Fuel-minimal Trajectory, Bottom: +5.0% fuel Noise-minimal Trajectory)

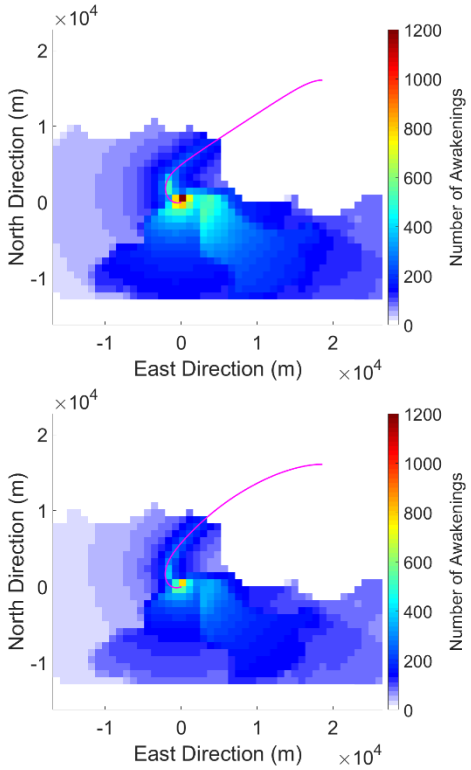

Figure A-2: Number of Awakenings Footprint for A320 (Top: +0.0% Fuel-minimal Trajectory, Bottom: +5.0% fuel Noise-minimal Trajectory)

- A332 Noise Footprint

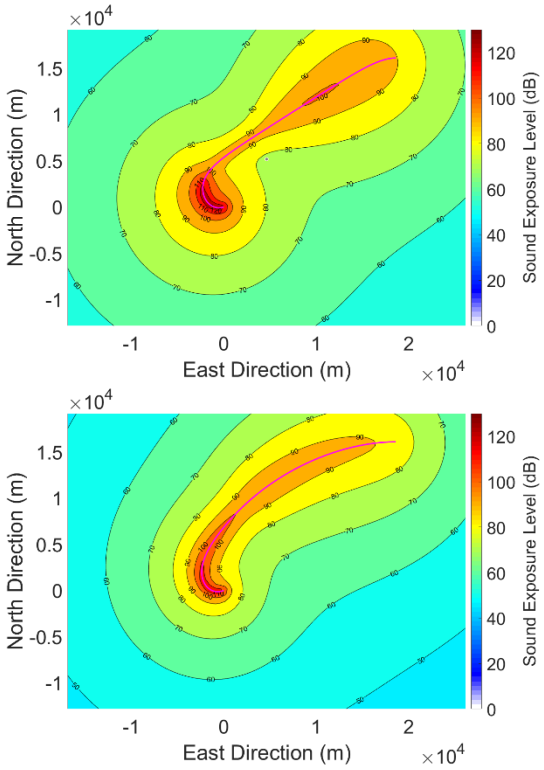

Figure A-3: Sound Exposure Level Footprint for A332 (Top: +0.0% Fuel-minimal Trajectory, Bottom: +5.0% fuel Noise-minimal Trajectory)

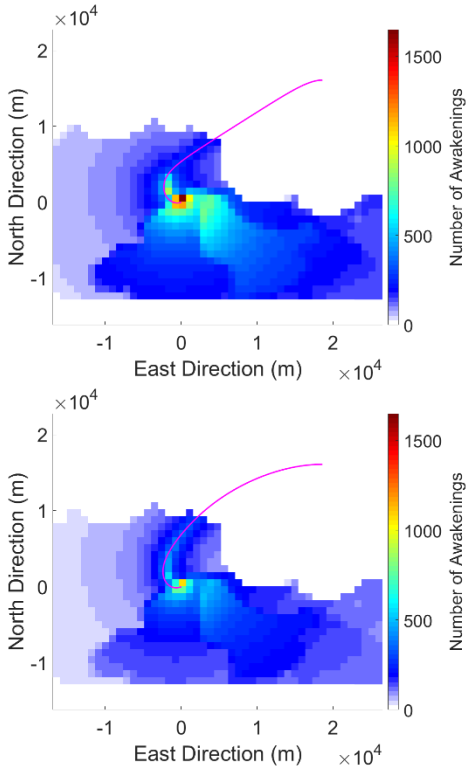

Figure A-4: Number of Awakenings Footprint for A332 (Top: +0.0% Fuel-minimal Trajectory, Bottom: +5.0% fuel Noise-minimal Trajectory)

- B735 Noise Footprint

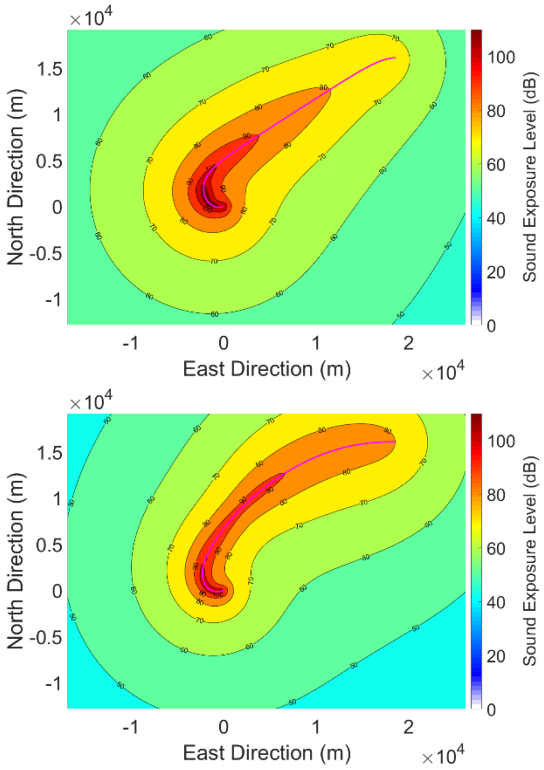

Figure A-5: Sound Exposure Level Footprint for B735 (Top: +0.0% Fuel-minimal Trajectory, Bottom: +5.0% fuel Noise-minimal Trajectory)

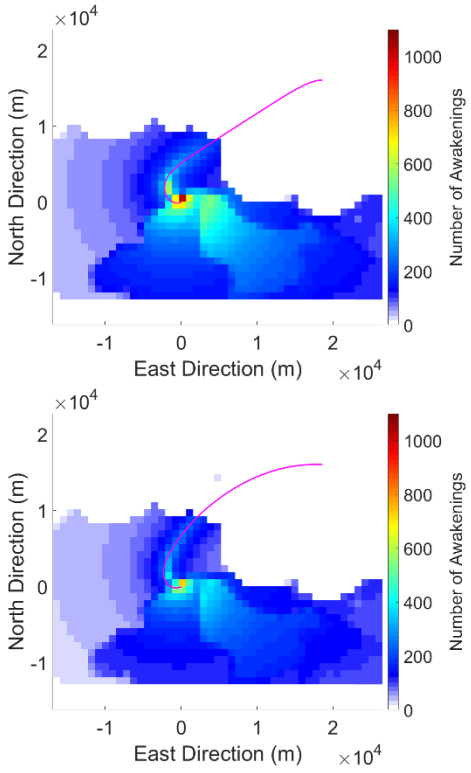

Figure A-6: Number of Awakenings Footprint for B735 (Top: +0.0% Fuel-minimal Trajectory, Bottom: +5.0% fuel Noise-minimal Trajectory)

- B738 Noise Footprint

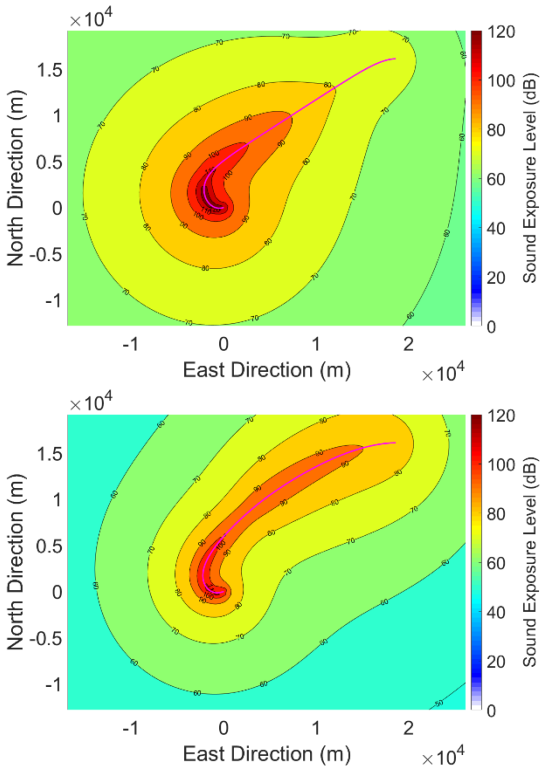

Figure A-7: Sound Exposure Level Footprint for B738 (Top: +0.0% Fuel-minimal Trajectory, Bottom: +5.0% fuel Noise-minimal Trajectory)

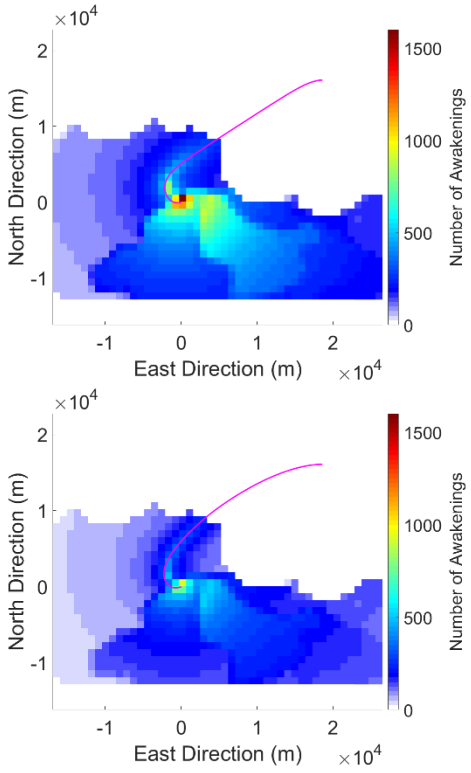

Figure A-8: Number of Awakenings Footprint for B738 (Top: +0.0% Fuel-minimal Trajectory, Bottom: +5.0% fuel Noise-minimal Trajectory)

- B773 Noise Footprint

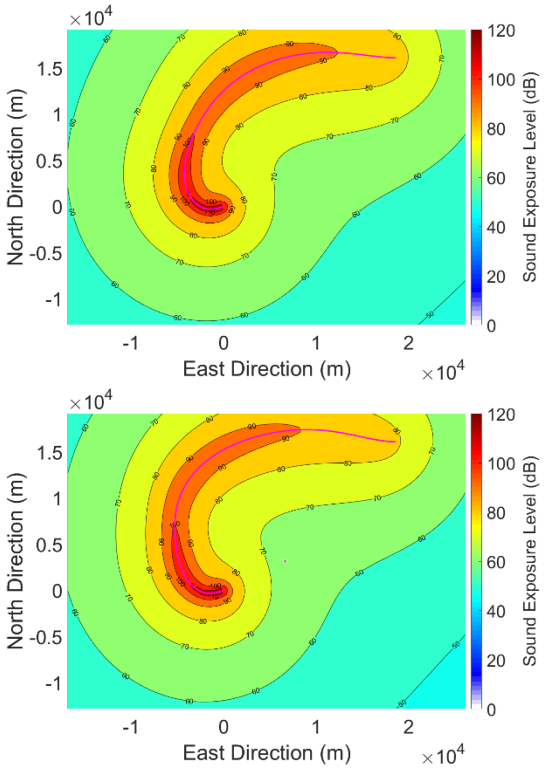

Figure A-9: Sound Exposure Level Footprint for B773 (Top: +0.0% Fuel-minimal Trajectory, Bottom: +5.0% fuel Noise-minimal Trajectory)

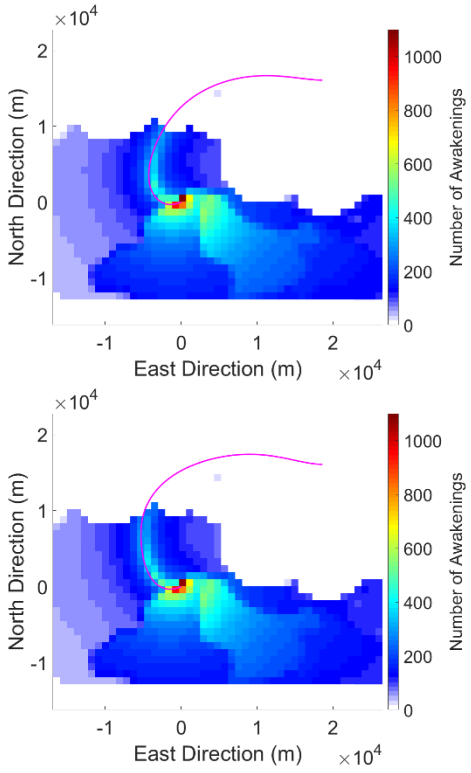

Figure A-10: Number of Awakenings Footprint for B773 (Top: +0.0% Fuel-minimal Trajectory, Bottom: +5.0% fuel Noise-minimal Trajectory)

- CRJ9 Noise Footprint

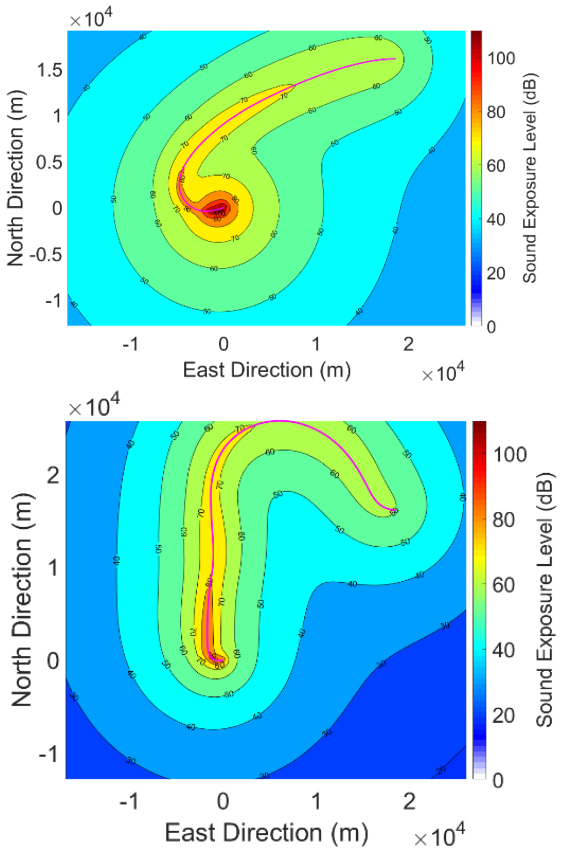

Figure A-11: Sound Exposure Level Footprint for CRJ9 (Top: +0.0% Fuel-minimal Trajectory, Bottom: +5.0% fuel Noise-minimal Trajectory)

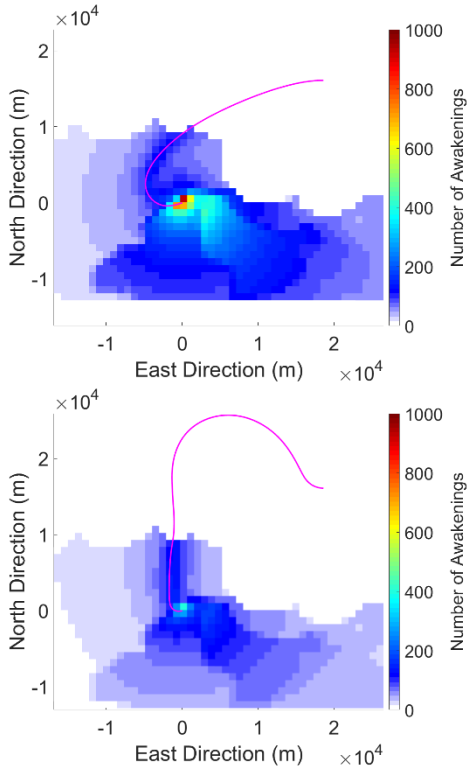

Figure A-12: Number of Awakenings Footprint for CRJ9 (Top: +0.0% Fuel-minimal Trajectory, Bottom: +5.0% fuel Noise-minimal Trajectory)